Local anaesthetic potential, Metabolic profiling, Molecular docking and In silico

ADME studies of *Ocimum forskolei*, Family *Lamiaceae*

Eman Maher Zahran[a], Usama Ramadan Abdelmohsen[a,b], Mahmoud. M. Shalash[C], M. Alaraby Salem[c], Hany Ezzat Khalil[d], Samar Yehia Desoukey[b], Mostafa Ahmed Fouad[b], Markus Krischke[e], Martin Mueller[e], and Mohamed Salah Kamel[b]

[a]Department of Pharmacognosy, Faculty of Pharmacy, Deraya University, Universities Zone, 61111 New Minia City, Egypt.

[b]Department of Pharmacognosy, Faculty of Pharmacy, Minia University, 61519 Minia, Egypt.

[c]Department of Pharmaceutical Chemistry, Faculty of Pharmacy, October University of Modern Sciences and Arts (MSA), Giza, Egypt.

[d]Department of Pharmaceutical Sciences, College of Clinical Pharmacy, King Faisal University, 31982, Al-Ahsa, Saudi Arabia.

[e]Julius-von-Sachs-Institute of Biosciences, Biocenter, Pharmaceutical Biology, University of Würzburg, Würzburg, Germany.

Corresponding author: Eman Maher Zahran, emanzahran84@yahoo.com

17

18

19

20

21

22

23

24

25

26

27 **Abstract**

28 The present study aimed to detect the bioactive metabolites from *Ocimum forskolei*

29 aerial parts which are responsible for the local anaesthetic activity of the ethyl

30 acetate fraction. Following a bioassay-guided fractionation, twelve compounds were

31 dereplicated from the ethyl acetate fraction which was the most potent one with a

32 mean onset of action (1.43±0.07****) min compared to tetracaine as a positive

33 control (1.37±0.07****) min. These compounds, along with seven other compounds

34 (isolated by diverse chromatographic techniques) were subjected to a molecular

35 docking study to declare the top scoring compounds predicted to be responsible for

36 such activity. The results highlighted Rabdosiin and Apigenin-7-O-rutinoside as the

37 main bioactive leaders of the local anaesthesia *via* forming multiple H- bonding with

38 the sodium ion channels leading to their blockade and loss of pain sensation, which

39 strongly supports the use of *O. forskolei* as a local anaesthetic agent.

42 **Experimental**

43 *Plant material*

44 Leaves and stems of *O. forskolei* were collected in September 2016 from the

45 National Garden of Jazan, KSA. Authentication of plant was established by Prof. Dr.

46 Mahmoud Abdelhady Hassan, Professor of Horticulture, Faculty of Agriculture, Minia

47 University. A voucher specimen (Mn-ph-Cog-038) was kept in the herbarium of

48 Pharmacognosy Department, Faculty of Pharmacy, Minia university, Minia, Egypt.

49 *Sample preparation*

50 The air dried, powdered leaves and stems (8 kg) were extracted by maceration with

51 95% ethanol at room temperature, yielding 400 g of crude extract which was

52 suspended in the least amount of distilled water to obtain an aqueous solution

53 successively partitioned with petroleum ether, dichloromethane (DCM), and ethyl

54 acetate using a separating funnel. The organic phase in each step was separately

55 evaporated under reduced pressure to afford the corresponding fractions: Fr.I (120

56 g), fr.II(35 g) and fr.III (32 g), respectively. The remaining mother liquor was then

concentrated to give the aqueous fraction fr.IV. All the resulting fractions were kept at 4º C for further phytochemical and biological investigations.

Animal model

This study was conducted on a population of fully grown *Bufo regularis* frogs (no attention is paid to weight or sex) in compliance with the guidelines for the care and use of laboratory animals of the National Institute of Health. Frogs were obtained from the pre-clinical animal house, faculty of medicine, Assuit university, Egypt, in which they were housed and bred under standardized conditions. They were allowed free access to food and drinking water. The animals were acclimatized to the environment for one week before commencement of the experiment. All conditions were also made to minimize animal suffering.

Acute toxicity (LD$_{50}$)

The acute toxicity of the total ethanol extract (TEE) was previously determined (Zahran et al. 2019).

Local anaesthetic study

The local anaesthetic activity of the TEE and its different fractions from *O. forskolei* Benth. was evaluated by the method described by Chakraborty et al. with slight modification where Tetracaine was used as the standard drug instead of Xylocaine (Chakraborty et al. 2010). The lumbar plexus anaesthesia model in *Xenopus laevis* frogs was used to determine the relative speed of onset of anaesthesia, instead of the wheel method performed on guinea pigs which is more suitable for estimating the degree of anaesthesia and its duration. Assessment of such former parameter is preferrable over the latter as such preparation undergoes constant deterioration. The frogs were divided into seven groups (five frogs each) which received the following treatment into the abdominal pouch *via* infiltration:

Group 1: -ve Control group, received 0.9 % saline.

Group 2: +ve Control group, received 2 % tetracaine

Group 3: Total ethanol extract group (20%).

Group 4: Petroleum ether fraction group (20%).

89   **Group 5:** Dichloromethane fraction group (20%).

90   **Group 6:** Ethylacetate fraction group (20%).

91   **Group 7:** Aqueous fraction group (20%).

92   They were decerebrated and upper parts of their spinal cords were destroyed down

93   to the level of the third vertebra using a pithing needle. The abdominal viscera were

94   excised and removed through a transverse incision made just below the sternum

95   thereby forming a pouch. The lumbar plexus was exposed carefully without

96   damaging it. The frogs were pinned to vertical boards with their legs hanging down.

97   The drugs were administered to the frogs in the different groups into the abdominal

98   pouch in sufficient volumes (20%) to submerge the lumbar plexus. The left and right

99   limbs of the frogs were immersed every minute for a maximum period of 10 s, to

100   avoid damaging the sensory nerve-endings by repeated application of stronger acid

101   than necessary in beakers containing 0.1(N) HCL and normal saline, respectively.

102   Afterwards the feet were rinsed in water. The time taken by the animals failing to

103   withdraw their feet from the acid beaker was recorded as the "onset of local

104   anesthetic action" (Chakraborty, et al. 2010)

105   **Statistical analysis** Data were expressed as mean ± S.E.M (n = 5). One-way analysis of

106   variance (ANOVA) followed by Dunnett's test was applied. Graph Pad Prism 5 was

107   used for statistical calculations (Graph pad Software, San Diego, California, USA).

108   Results were regarded as significant as follows: $*P<0.05$, $**P<0.01$, $***P<0.001$,

109     $****P<0.0001$ (Table S1).

110   ***LC-HR-MS analysis***

111   Acquity Ultra Performance Liquid Chromatography system coupled to a Synapt G2

112   HDMS quadrupole time-of-flight hybrid mass spectrometer (Waters, Milford, USA).

113   Chromatographic separation was carried out on a BEH C18 column (2.1 × 100 mm,

114   1.7 μm particle size; Waters, Milford, USA) with a guard column (2.1 x5 mm, 1.7 μm

115   particle size) and a linear binary solvent gradient of 0%–100% eluent B over 6 min at

116   a flow rate of 0.3 mL min−1, using 0.1% formic acid in water (v/v) as solvent A and

117   acetonitrile as solvent B. The injection volume was 2 μL and the column temperature

118   was 40°C. To convert the raw data into separate positive and negative ionization

119   files, Ms converter software was used Using MZmine 2.12 as framework for MS data

120   differential analysis were, the raw data were imported by selecting the

121 ProteoWizard-converted positive or negative files in mzML format (Tawfike et al.
122 2019) (Ibrahim et al. 2018). **(**DNP and METLIN databases were used for dereplicating
123 each *m/z* ion peak (using RT and *m/z* threshold of ±5 ppm), which provided the
124 putative identities of all metabolomes in the total extract (s) in details (Elsayed et al.
125 2018)

126

127 ***Phytochemical study (Isolation and purification of compounds)***
128 A part of the ethyl acetate fraction was subjected to VLC fractionation on a silica gel
129 column. Elution was performed using DCM-MeOH gradient mixtures in the order of
130 increasing polarities (20, 30, 40, 50 and 100%). The effluents were collected in
131 fractions (100 ml each); each fraction was concentrated and monitored by TLC.
132 Similar fractions were grouped together and concentrated under reduced pressure
133 to provide four major fractions (I - IV). Fraction I (1.4 g) was further fractionated on a
134 silica gel column (CC) using DCM-MeOH gradient mixtures to yield four subfractions
135 (I-1, I-2, I-3 & I-4). Subfraction I.1 (140 mg) was fractionated on silica gel CC followed
136 by paper chromatography to yield compound **13** (15 mg). Fraction III (3 g) was
137 subjected to silica gel CC employing gradient elution with DCM-MeOH and the
138 effluents were collected in fractions (500 ml each) providing 5 subfractions (III-1 – III-
139 5). Compound **14** (25 mg) was isolated from subfraction III-1 (170 mg) using silica gel
140 CC with DCM-MeOH 6-4 isocratic elution. Compounds **15** (17 mg) and **16** (9 mg)
141 followed the same behaviour and were isolated from subfraction III-2 (110 mg) with
142 DCM-MeOH 5-5 isocratic elution. Subfraction III-3 (2.1 g) yielded compounds **17** (6
143 mg) and **18** (2.3 mg) employing EtOAc-MeOH gradient elution on different silica gel
144 columns. Subfraction III-4 gave compound **19** (15 mg). All compounds were
145 identified by different NMR spectroscopic analysis and comparison with literature
146 (Figure 2B, S2 – S8).

147 ***ADME-toxicity***
148 It was predicted for the most active compounds using the online platform of
149 SwissADME (Daina et al. 2017). The summary of data is provided in Table S3.

150 ***Molecular docking analysis***
151 Sodium channels located on cell membranes and involved in pain sensation *via*
152 neuro transmission are used to study the local anaesthetic action of our compounds.

153   The docking analysis in brief was concerned with the protein structure of the sodium

154   channel and its active site which where adopted based on the work of Tikhonov and

155   Zhorov (Tikhonov et al. 2017). Visualization and docking were performed using the

156   MOE software (CCGI 2016) with default parameters for rigid-body docking. Docking

157   was performed for the 19 compounds identified in the extract, as well as for

158   tetracaine and lidocaine as standards, and their docking scores were provided in

159   Table S4.

160   **Results and discussion**

161   The results mentioned in Table S1 clearly showed that all the different fractions

162   together with the TEE significantly exhibited a local anaesthetic action following the

163   lumbar plexus anaesthesia model in frogs, and this effect persisted over the whole

164   observation period (30 min). The ethyl acetate fraction was the highest significant

165   one with a mean onset of action of 1.43+-0.07****min in comparison with

166   tetracaine   1.37 +- 0.07**** min. The ethyl acetate fraction was followed by both

167   the aqueous and the TEE with mean onset of action of 1.70±0.07**** and 5.77±

168   0.4****; respectively; while both Pet. ether and DCM fractions exhibited a delayed

169   action but still significant with mean onset of 19.67+- 0.33** and 18.67+- 0.67**,

170   respectively.

171   The LC-HR-MS-coupled metabolomic analysis led to identification of 12 different

172   compounds with the predominance of phenolic compounds. The dereplicated

173   compounds which are common among different *Lamiaceous* species are listed in

174   Table S2 with thier relevant data.

175   The phytochemical study resulted in the isolation and identification of 7 compounds;

176   most of them are flavonoids and flavonoid glycosides together with the presence of

177   two caffeic acid derivatives (Figure 2 A & B). They were identified as acacetin which

178   was previously isolated from *O. sanctum* leaves (Gomes et al. 2011) as well as methyl

179   rosmarinate and methyl caffeate which were previously isolated from *O. basilicum*

180   roots (Singh et al. 2018). Didymin was detected in *Clinopodium mexicanum* (Estrada-

181   Reyes et al. 2010) and apigenin-7-O-rutinoside was previously isolated from

182   *Origanum vulgare* (Martins et al. 2014). Prunin was detected in many *Thymus* plants

183   (Leal et al. 2017) while acacetin-7-O-glucoside was precipitated in leaf tissues of

184   different *Mentha* species (Mimica-Dukic et al. 2008).

185 The molecular docking analysis was performed in an attempt to explain the observed

186 local anaesthetic activity of the ethyl acetate fraction and all docking scores were

187 reported in Table S4.

188 The compounds were investigated based on their scores and visual inspection of the

189 formed interactions. As shown in figure S9, the active site of the sodium channel is

190 buried in the inner-pore region of the alpha-subunit which is lined by the S6 helix

191 and the p-loop. Within the active site, there are several hydrophobic amino acids,

192 including Phe 315 and Phe 249 with the propensity of π stacking. There are also

193 potential H-bond donors like Lys 250 and Gln 249 along with Ser 315 and Thr 247,

194 which= can also act as acceptors.

195 The interactions formed with the active site of the voltage-gated sodium channel

196 and the two top scoring compounds, rabdosiin and apigenin-7-O-rutinoside, are

197 illustrated in figure 3. Upon examination of the results, it was found that both

198 compounds formed hydrogen bonds as well as arene-H interactions with the sodium

199 channels and these two types of interactions were strong enough to stabilize both

200 compounds in the docked pose. Rabdosiin formed five interactions, two hydrogen

201 bonds; attached to the phenyl rings; with Cys 248 and Ser 315, one hydrogen bond

202 belonging to a carboxylic group which interacted with Thr 248 and the last one

203 through an arene-H interaction with Gln 315 *via* the phenyl ring. Apigenin-7-O-

204 rutinoside formed three interactions with the ion channel, a hydrogen bond *via* the

205 hydroxyl group of glucose moiety with Cys 248, another binding of Asn 315 with the

206 rhamnose moiety and the third one through an arene-H interaction with Leu 319. On

207 the other hand, the analysis of the interactions formed by lidocaine in the binding

208 site of the ion channel showed that it formed similar interactions as the two top

209 scoring compounds expressed in a hydrogen bond between the amide carbonyl

210 group and Gln 249, as well as a π-π stacking *via* the phenyl ring of the ligand.

211 Comparing the docking poses of rabdosiin and apigenin-7-O-rutinoside with that of

212 lidocaine, it was found that the three compounds occupied the same binding pocket

213 although rabdosiin and apigenin-7-O-rutinoside occupied a larger volume of the

214 pocket, which might account for their superior binding scores. All the previous

215 results show both compounds to be the main responsible for the local anaesthetic

216 action of the ethyl acetate fraction.

217

218

219

Table S1: Results of local anaesthetic activity of the TEE and different fractions of *O. forskolei*. On plexus anaesthesia in frogs

Group	Drug	Onset of local anaesthetic action (mean ±SEM) (min)
-ve control	0.9 % saline	22.00 ± 0.00
+ve control	2% tetracaine	1.37 ± 0.07****
TEE	20 %	5.77 ± 0.40****
Petroleum ether fr.	20 %	19.67± 0.33**
DCM fr.	20 %	18.67± 0.67**
Ethyl acetate fr.	20 %	1.43±0.07****
Aqueous fr.	20 %	1.70±0.07****

222

Table S2. A list of dereplicated compounds by metabolomic analysis from ethyl acetate fraction of *O. forskolei*

Compound	Acc. Mass	*m/z*	Mol. formula	Source and Reference
Rabdosiin	718.15	718.15	$C_{36}H_{30}O_{16}$	*Ocimum basilicum* (Flegkas et al. 2019)
Protocatechuic acid	154.03	154.03	$C_7H_6O_4$	*Ocimum basilicum* (Bilal et al. 2012)
Methyl gallate	184.04	184.03	$C_8H_8O_5$	*Ocimum sanctum* (Mondal et al. 2009)
Tournefolic acid B	312.27	312.22	$C_{17}H_{12}O_6$	*Clinipodium chinense* (Yu et al. 2019)
Chlorogenic acid	353.08	353.10	$C_{16}H_{18}O_9$	*Ocimum basilicum*, (Shoeb et al. 2007)
Citrusin C	326.14	326.12	$C_{16}H_{22}O_7$	*Ocimum sanctum* (Suzuki et al. 2009)

Salvianolic acid F	314.08	314.07	$C_{17}H_{14}O_6$	*Melissa officinalis* (Barros et al. 2013)
Dehydrodieugenol B	326.15	327.16	$C_{20}H_{22}O_4$	*Ocimum sanctum* (Suzuki, et al. 2009)
Lithospermic acid	538.1	537.1	$C_{27}H_{22}O_{12}$	*Ocimum basilicum* (Tada et al. 1996)
Orientin	448.1	447.09	$C_{21}H_{20}O_{11}$	*Ocimum sanctum* (Sharma et al. 2016)
Rutin	610.35	609.15	$C_{27}H_{30}O_{16}$	*Ocimum kilimandscharicum* (Grayer et al. 2002)
Rosmanol	344.42	345.17	$C_{20}H_{28}O_5$	*Salvia pachyphylla* (Guerrero et al. 2006)

225

226
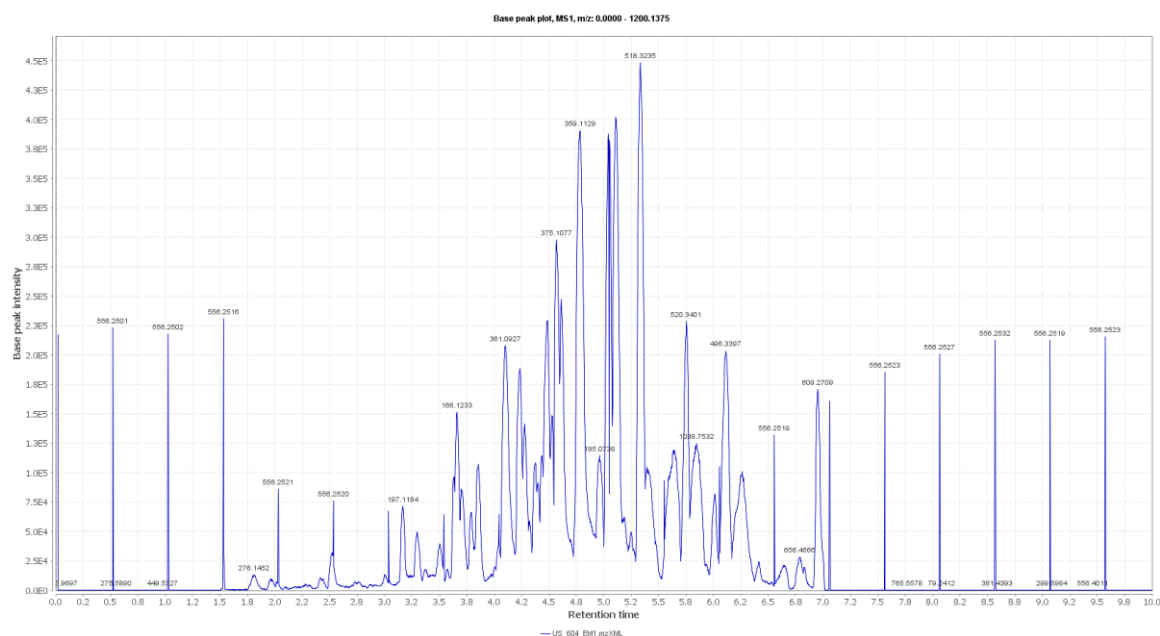
227

228   **Figure S1:** Total ion chromatogram of the ethyl acetate fraction of *O. forskolei*
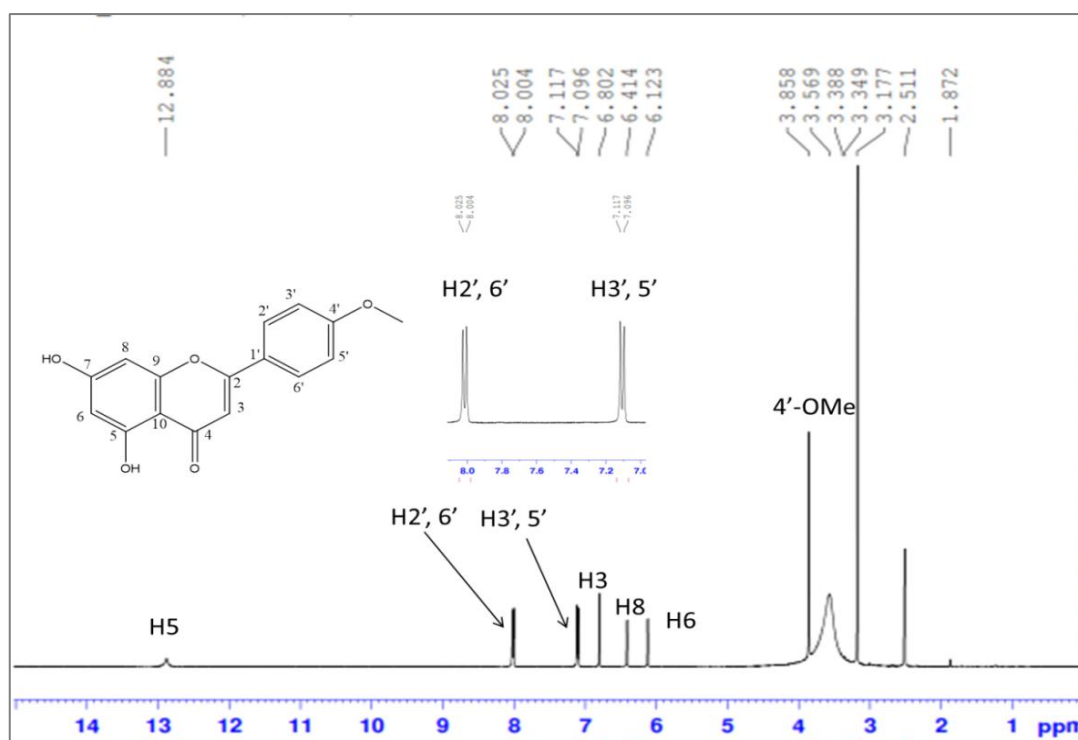
Figure S2.A: ^{1}H-NMR spectrum of acacetin (DMSO-d$_6$, 400 MHz)
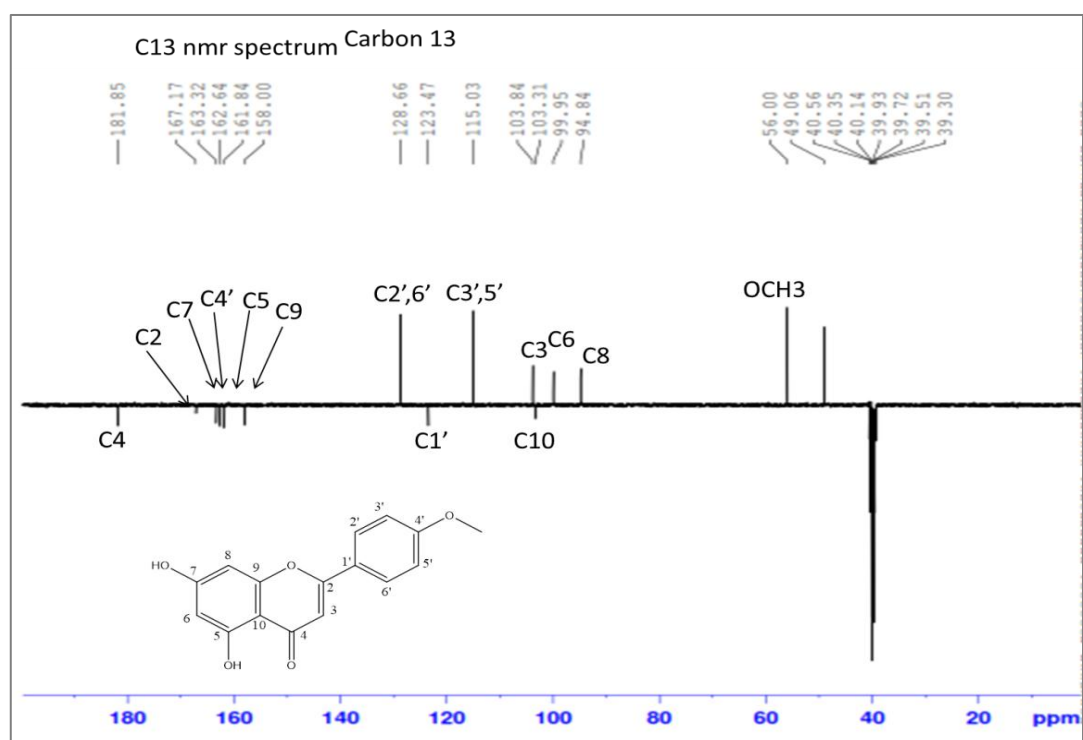
Figure S2.B: DEPT-Q spectrum of acacetin (DMSO-d$_6$, 100 MHz)
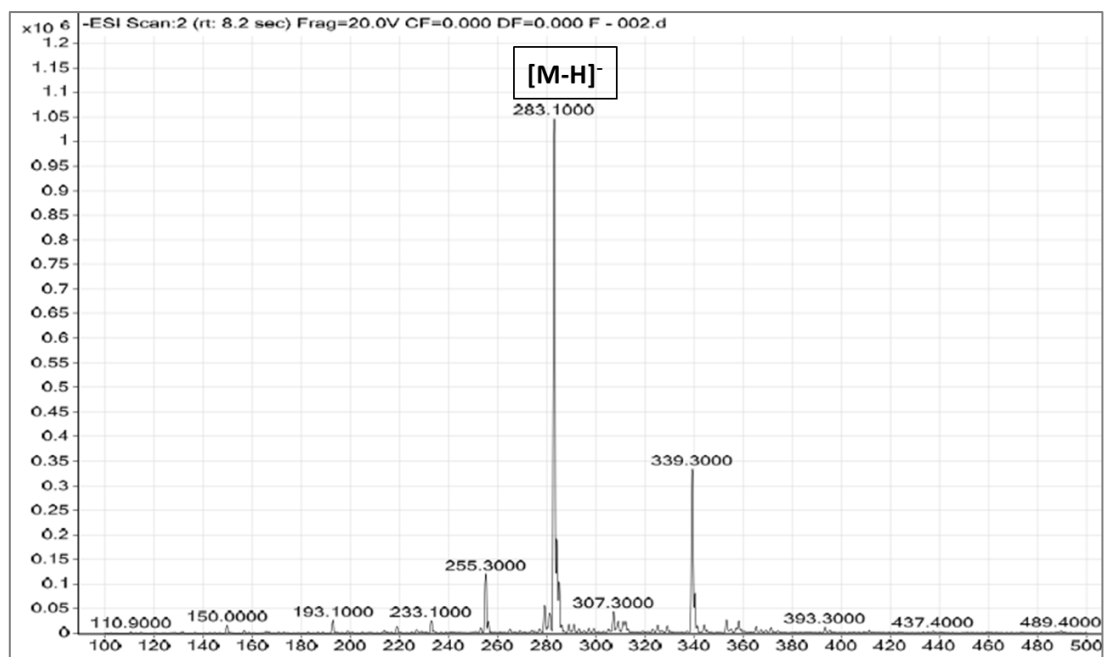
Figure S2.C: ESI-MS spectrum of acacetin
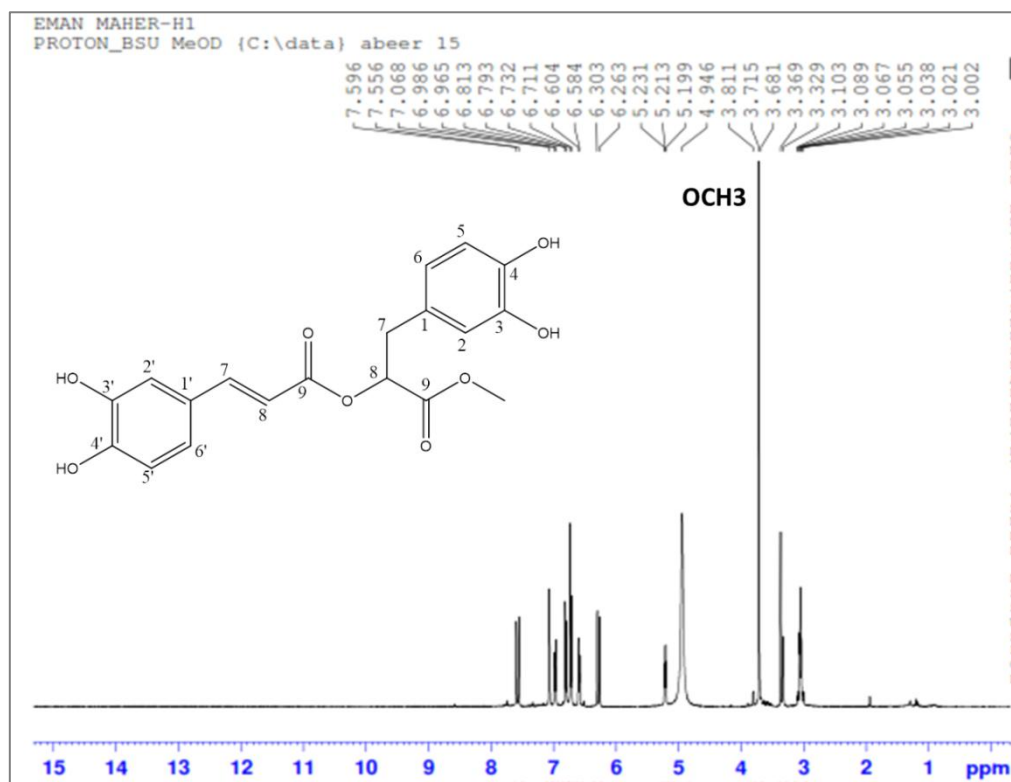
Figure S3.A: ^{1}H-NMR spectrum of methyl rosmarinate (CD$_3$OD, 400 MHz)
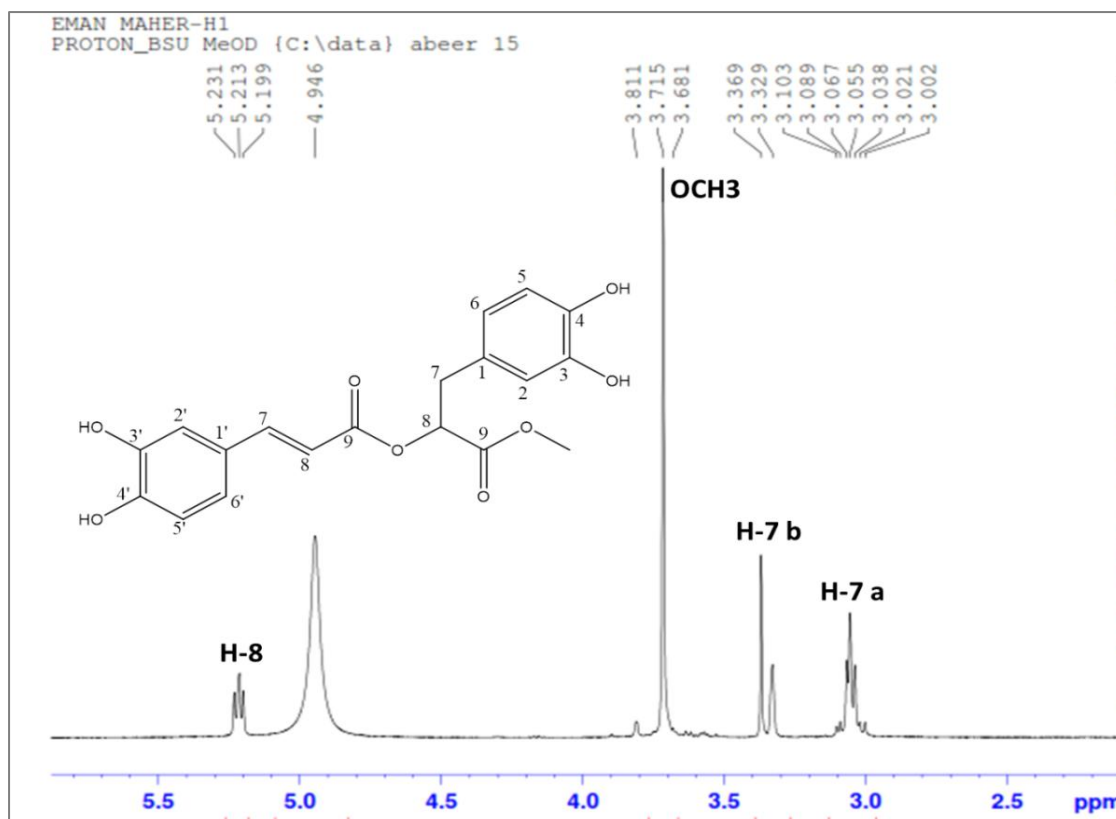
Figure S3.B: Expanded ^{1}H-NMR spectrum of methyl rosmarinate (CD$_3$OD, 400 MHz)
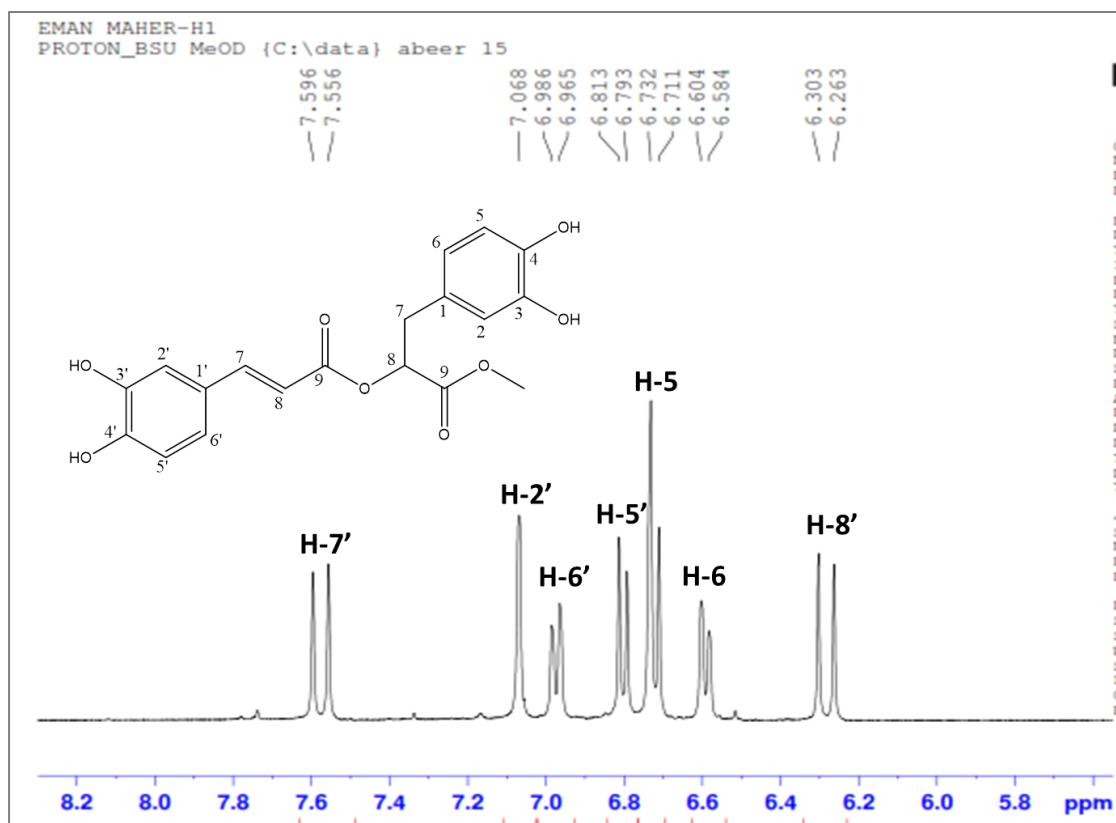
Figure S3.C: Expanded ^{1}H-NMR spectrum of methyl rosmarinate (CD$_3$OD, 400 MHz)
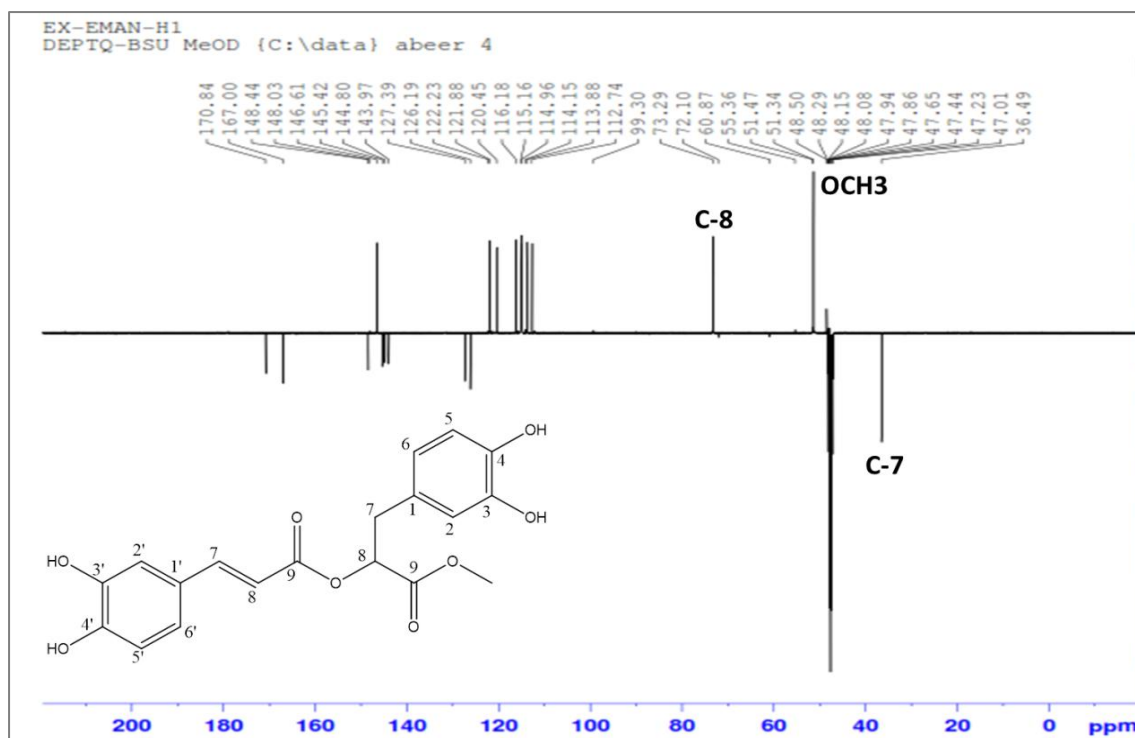
Figure S3.D: DEPT-Q spectrum of methyl rosmarinate (CD$_3$OD, 100 MHz)
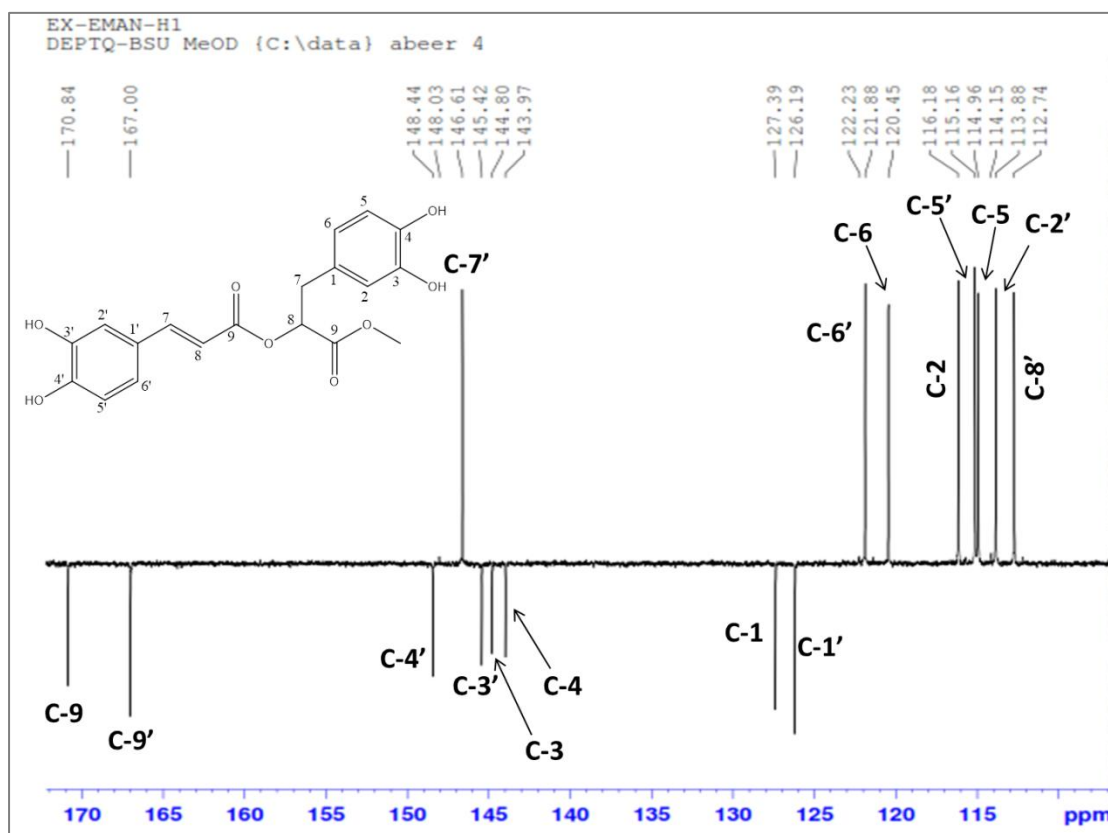
Figure S3.E: Expanded DEPT-Q spectrum of methyl rosmarinate (CD$_3$OD, 100 MHz)
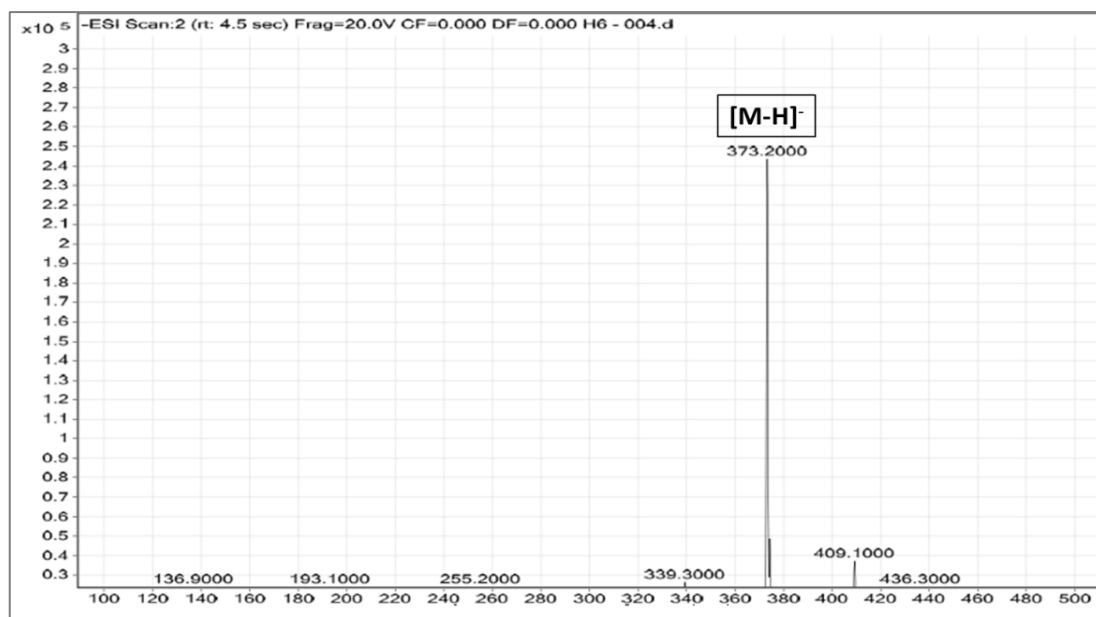
Figure S3.F: ESI-MS of methyl rosmarinate
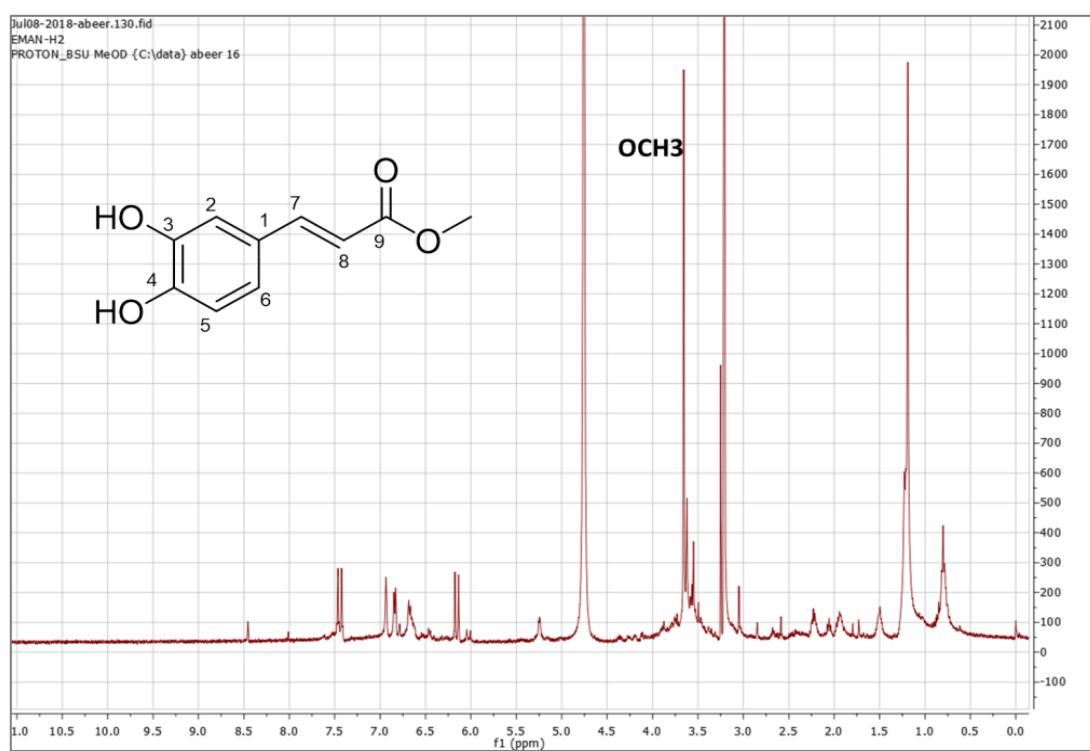
Figure S4.A: ^{1}H-NMR spectrum of methyl caffeate (CD$_3$OD, 400 MHz)
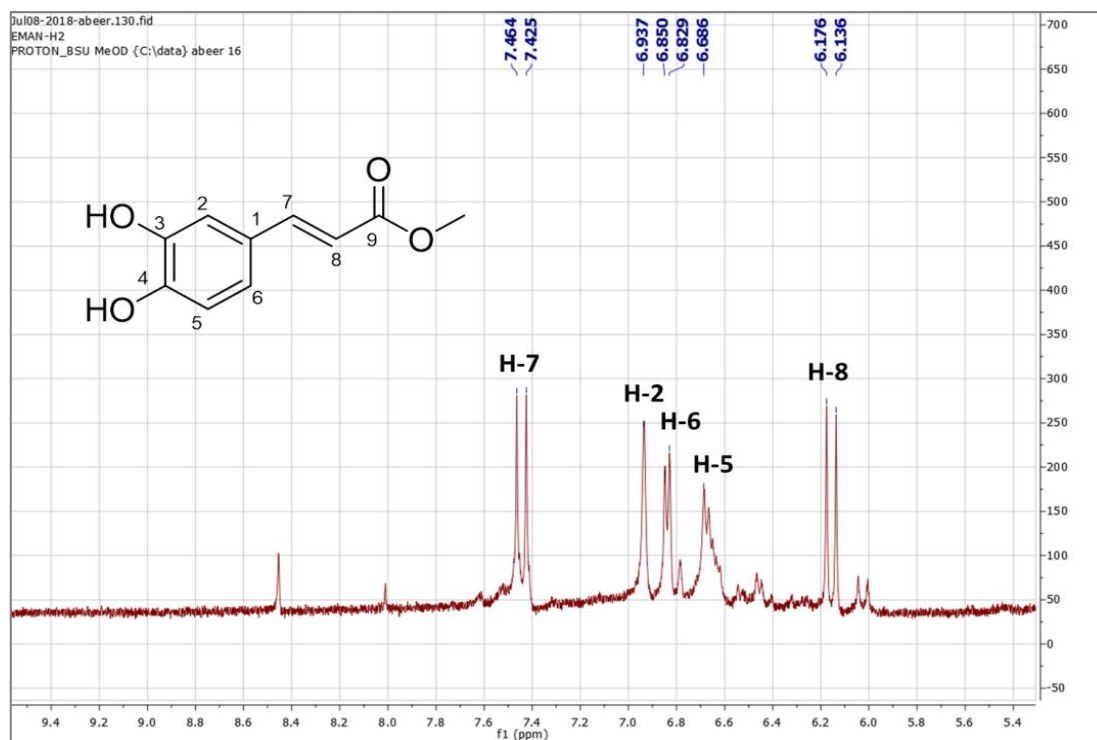
Figure S4.B: Expanded ^{1}H-NMR spectrum of methyl caffeate (CD$_3$OD, 400 MHz)
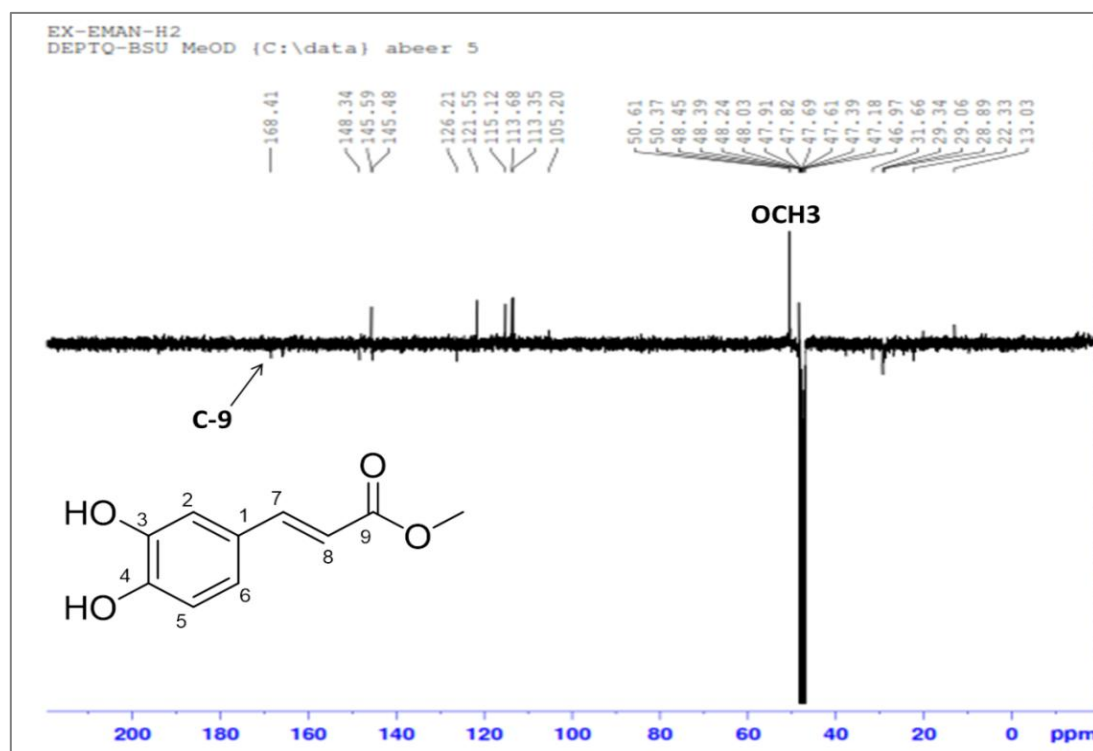
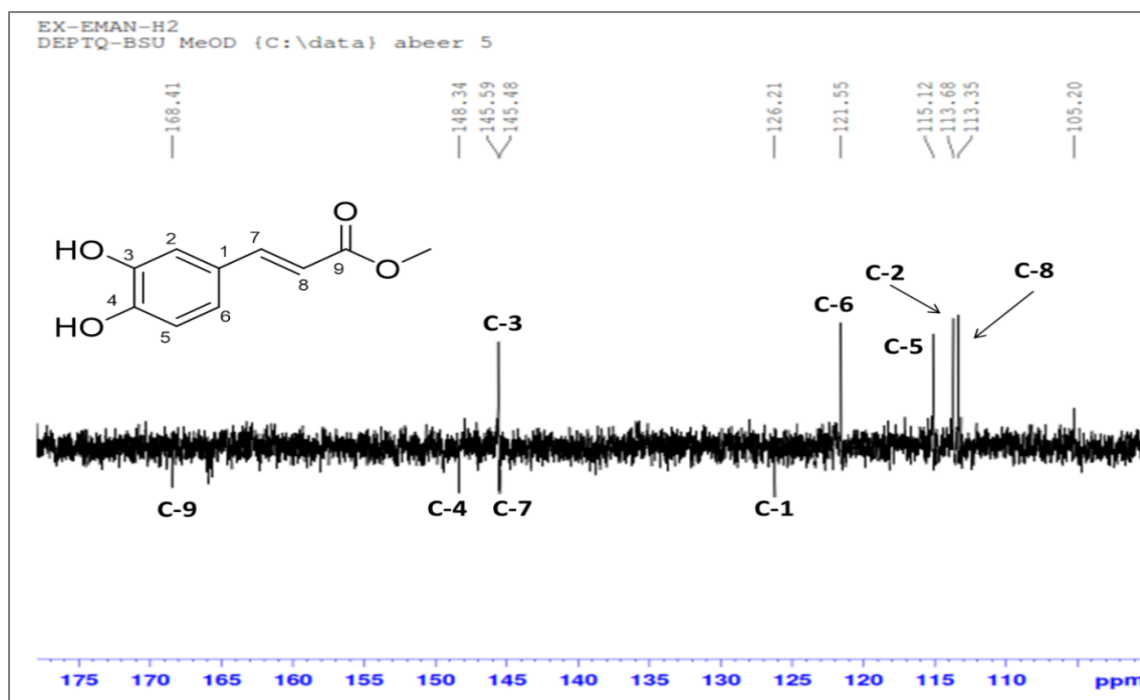Figure S4.C: DEPT-Q spectrum of methyl caffeate (CD$_3$OD, 100 MHz)

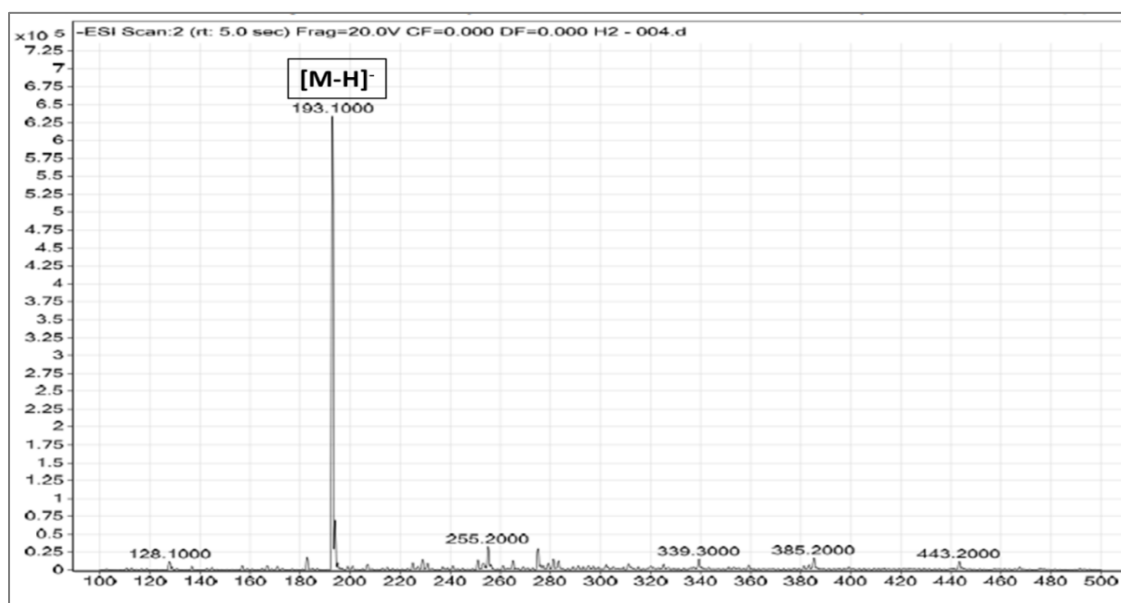**Figure S4.D:** Expanded DEPT-Q spectrum of methyl caffeate (CD$_3$OD, 100 MHz)

255

256

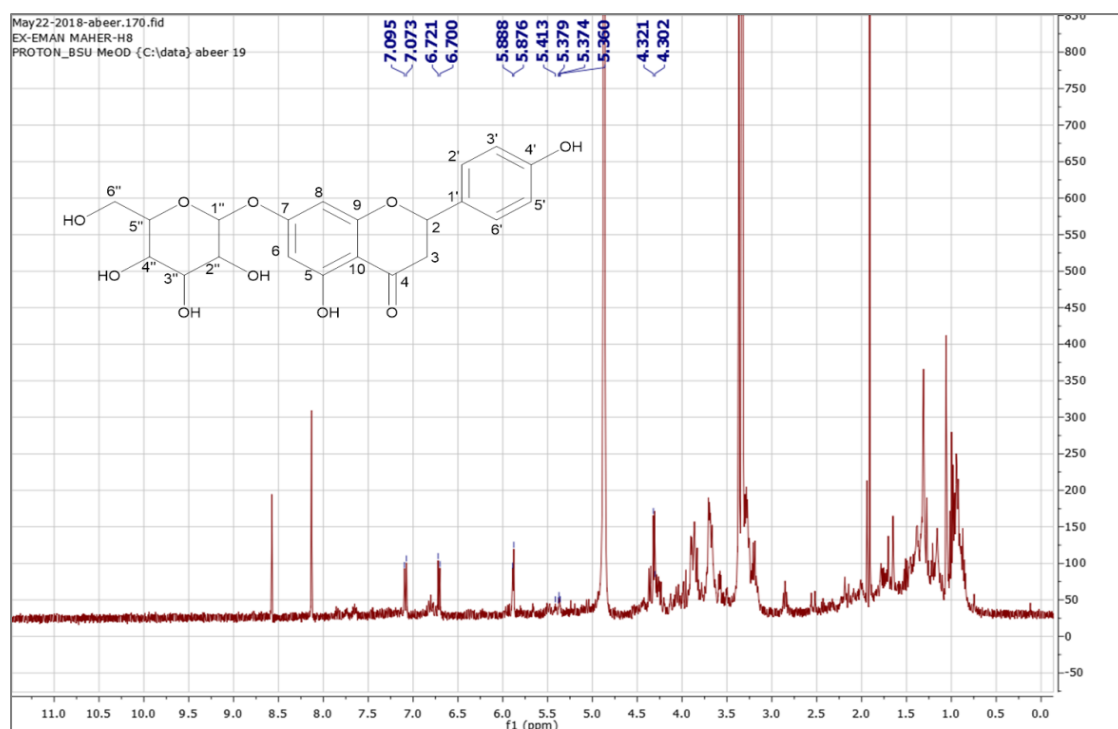**Figure S4.E:** ESI-MS of methyl caffeate

257

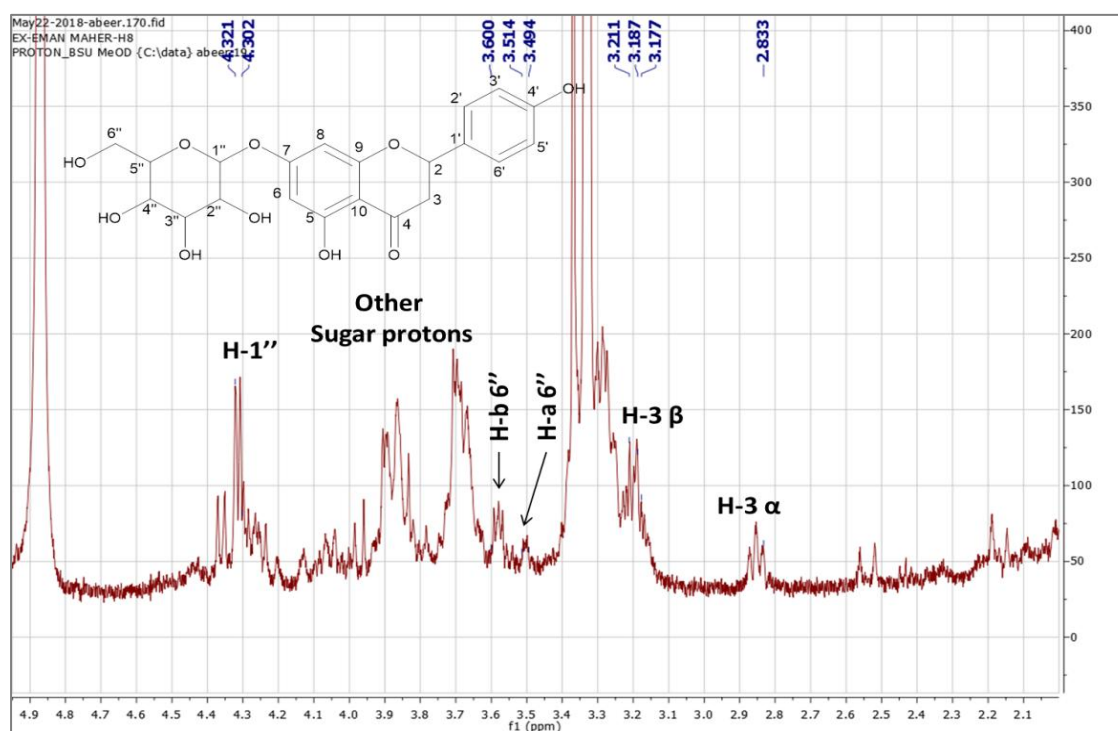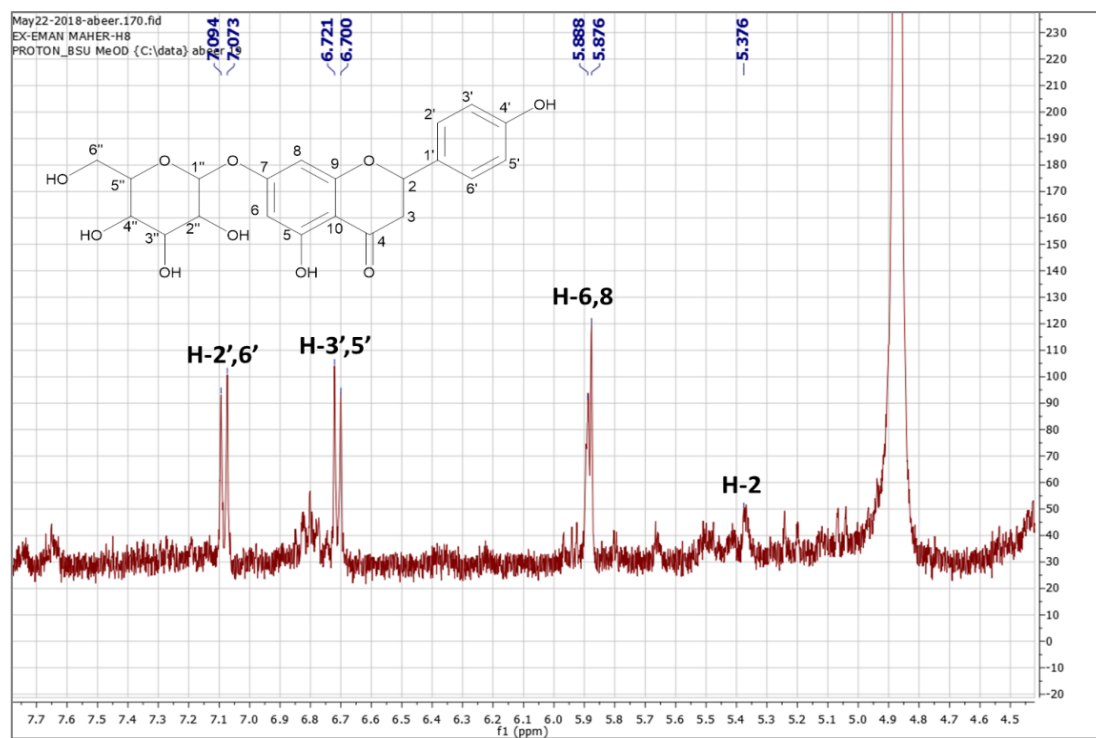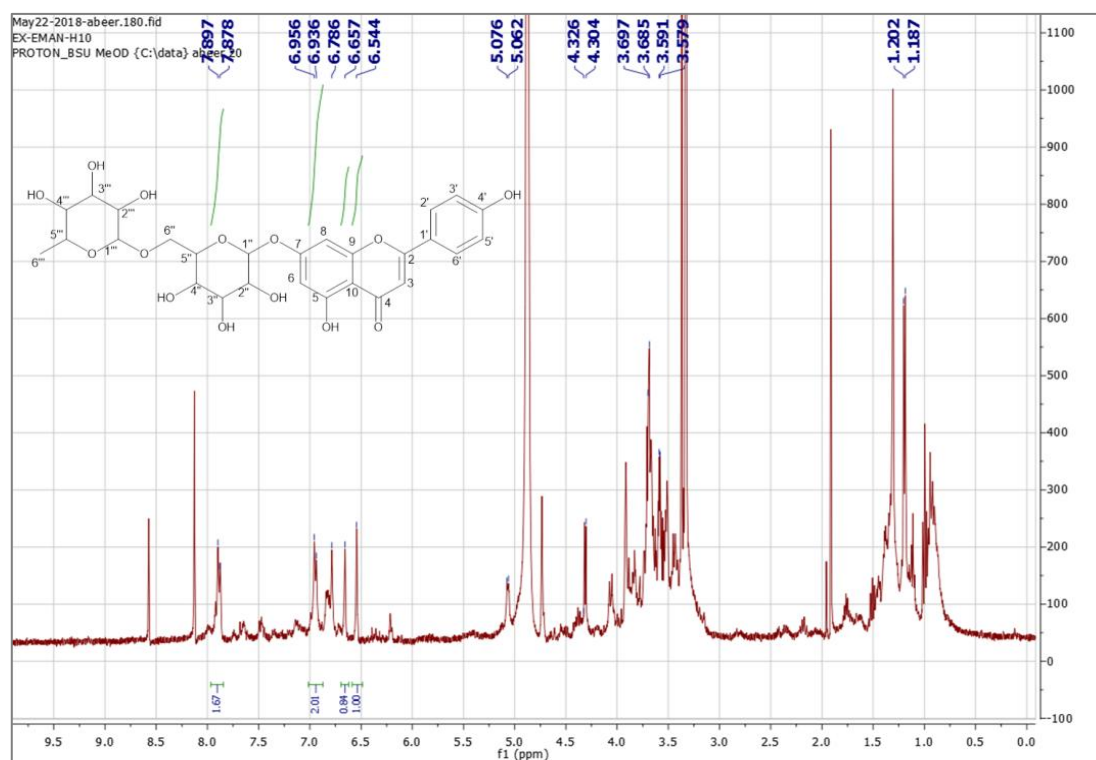**Figure S5.A:** ^{1}H-NMR spectrum of Prunin (CD$_3$OD, 400 MHz)

Figure S5.B: Expanded ^{1}H-NMR spectrum of Prunin (CD$_3$OD, 400 MHz)

Figure S5.C: Expanded ^{1}H-NMR spectrum of Prunin (CD$_3$OD, 400 MHz)

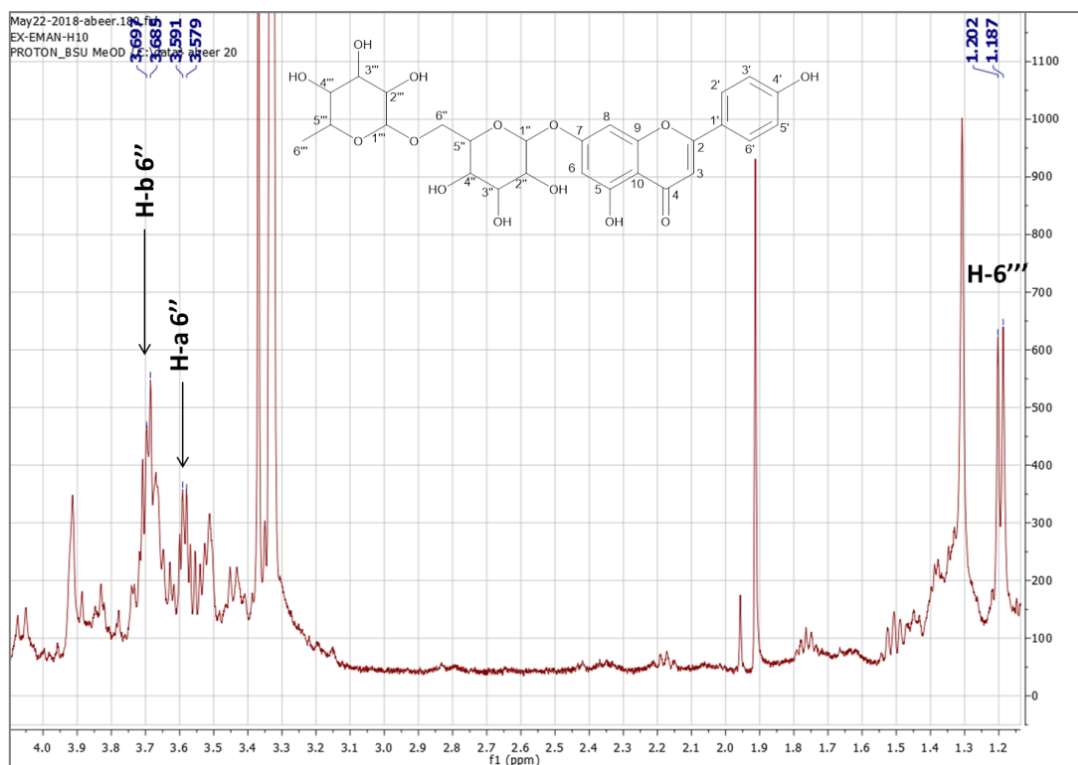**Figure S6.A.** ^{1}H-NMR spectrum of Apigenin-7-O-rutinoside (CD$_3$OD, 400 MHz)

Figure S6.B: Expanded ^{1}H-NMR spectrum of Apigenin-7-O-rutinoside (CD$_3$OD, 400 MHz)
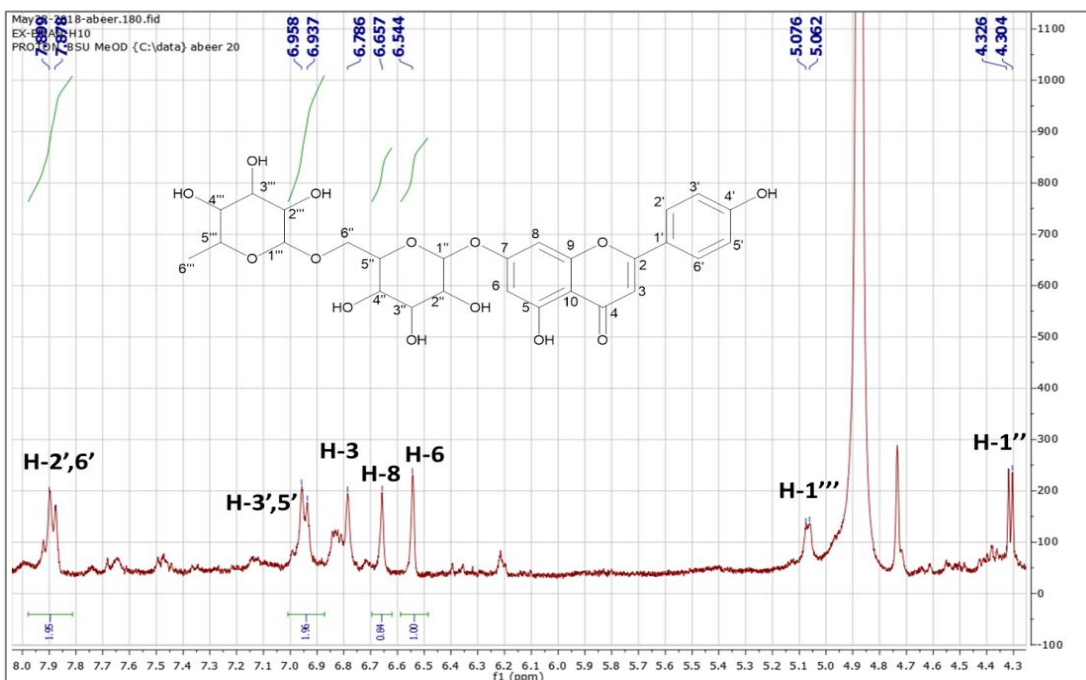

Figure S6.C: Expanded ^{1}H-NMR spectrum of Apigenin-7-O-rutinoside (CD$_3$OD, 400 MHz
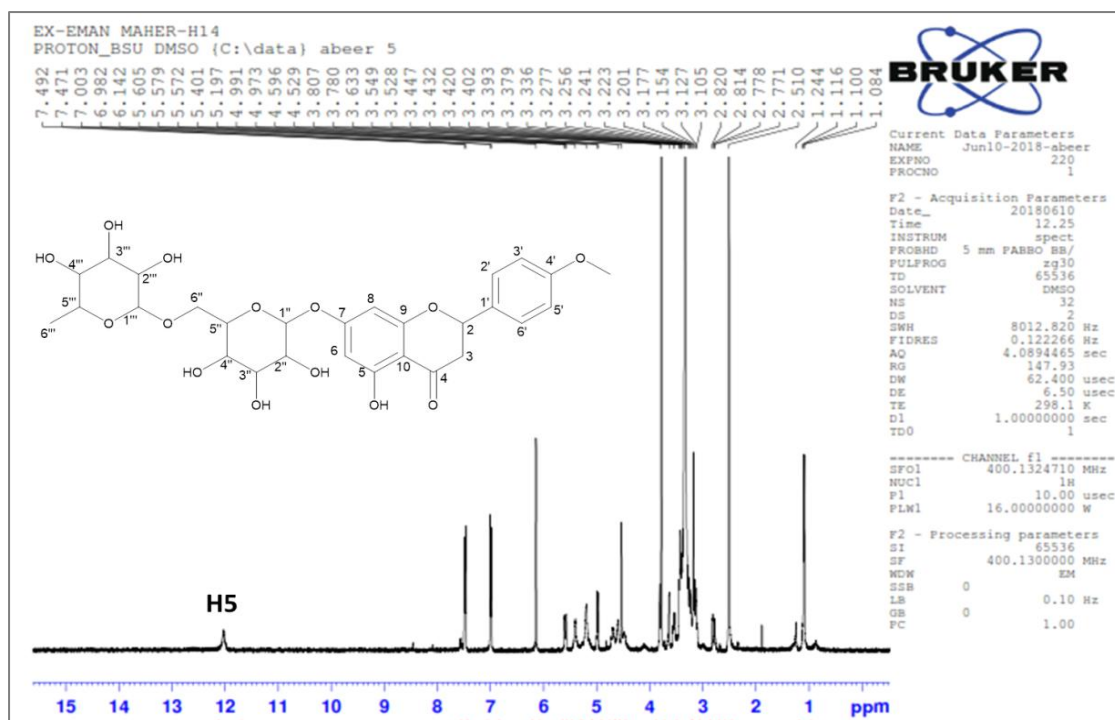
Figure S7.A: ^{1}H-NMR spectrum of Didymin (CD$_3$OD, 400 MHz)

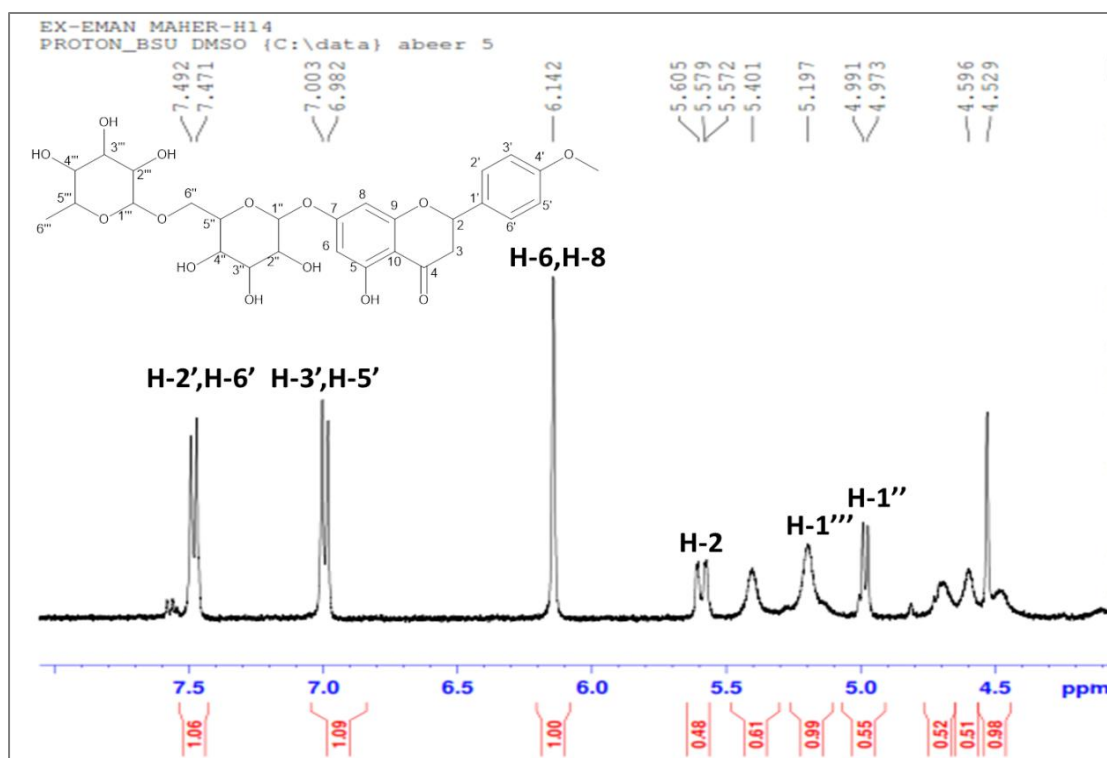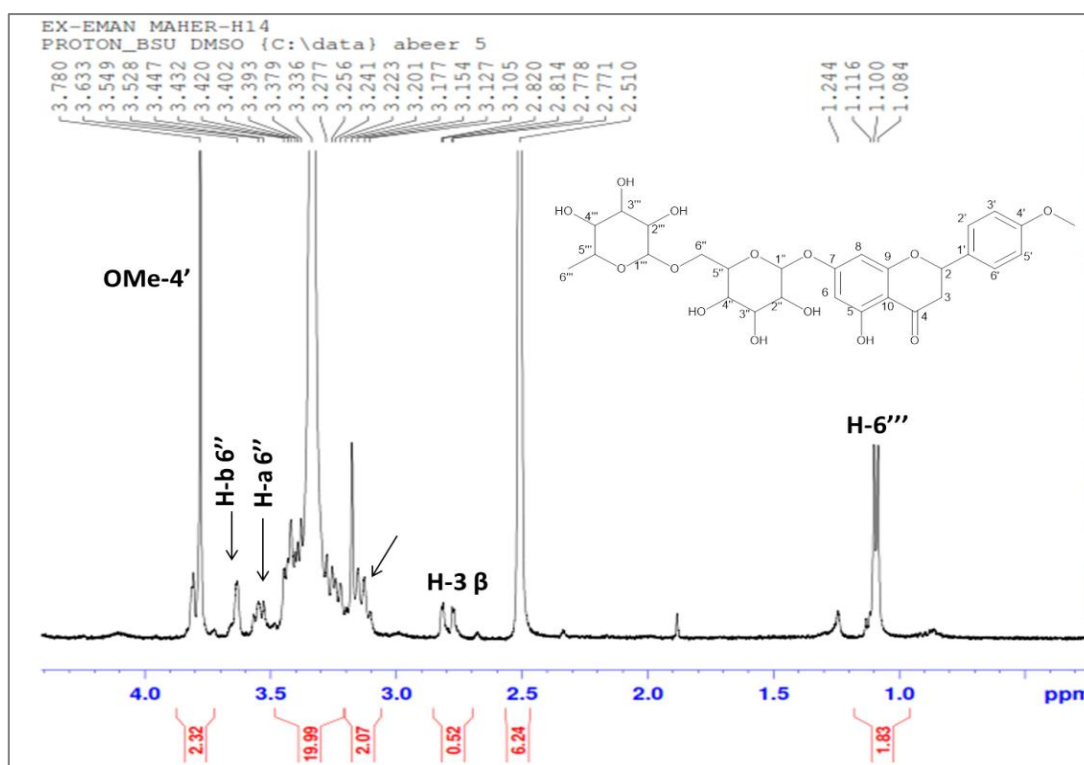Figure S7.B: Expanded ^{1}H-NMR spectrum of Didymin (CD$_3$OD, 400 MHz)

Figure S7.C: Expanded ^{1}H-NMR spectrum of Didymin (CD$_3$OD, 400 MHz)
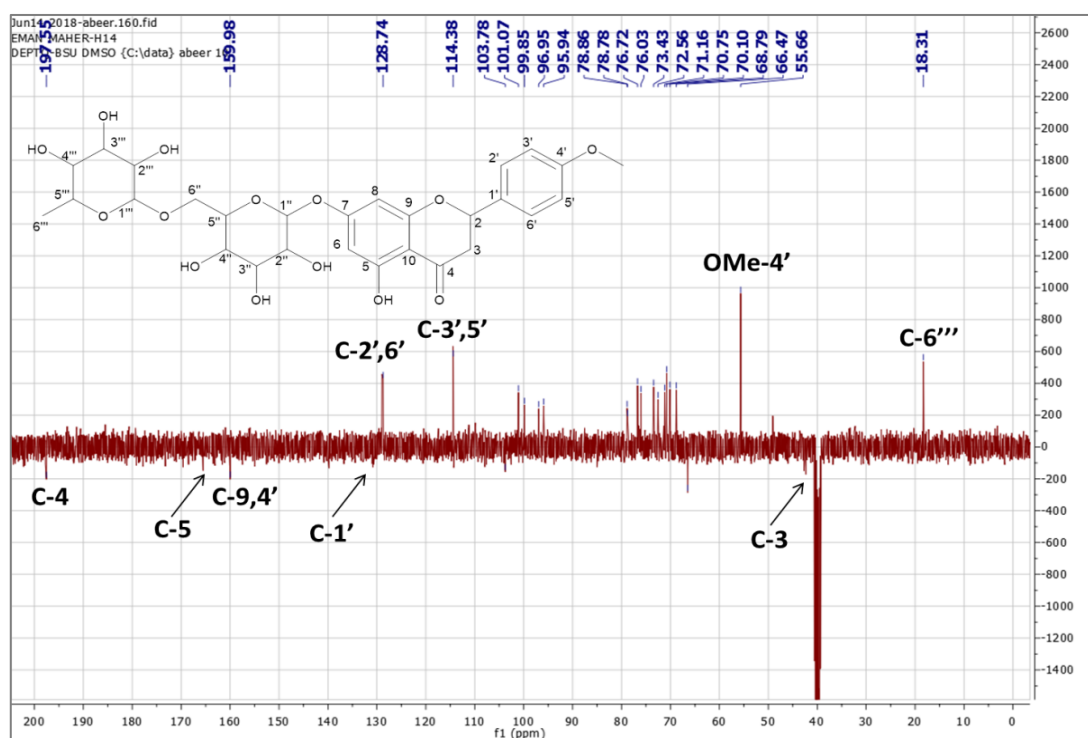

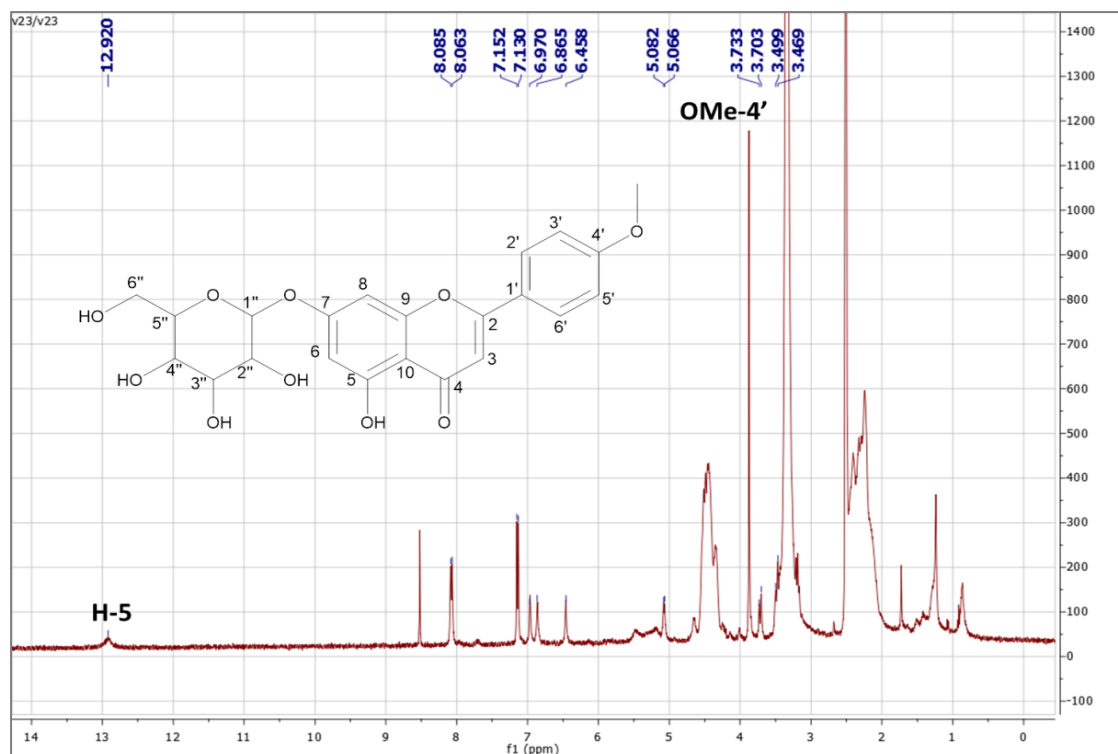**Figure S7.D:** DEPT-Q spectrum of Didymin (CD$_3$OD, 100 MHz)

Figure S8.A: ^{1}H-NMR spectrum of Acacetin-7-O-glucoside (DMSO-d$_6$, 400 MHz)
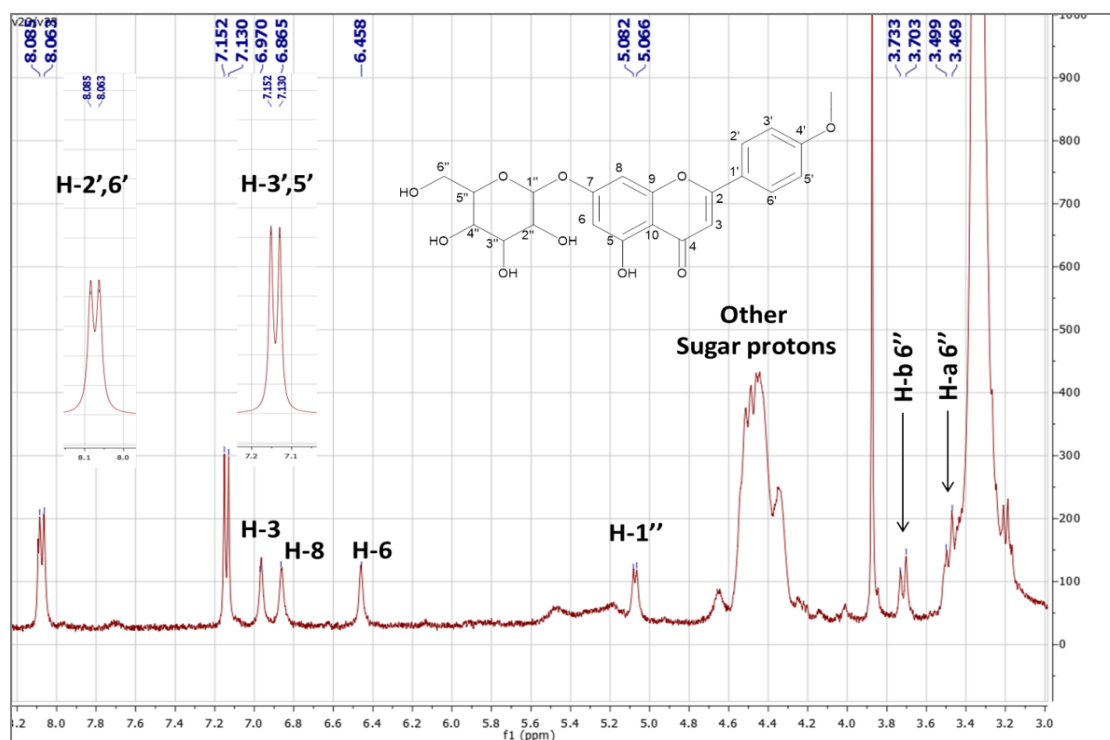

Figure S8.B: Expanded ^{1}H-NMR spectrum of Acacetin-7-O-glucoside (DMSO-d$_6$, 400 MHz)

287 **Table S3: summary of predictions made by SwissADME web tool for the isolated compounds from *O. forskolei* Benth.**

Cp.	Fr. C3	R.b	TPSA	XLOGP3	E. L	GI abs.	BBB P.	L.v.	B.s.	P.a	B.a	Cy
1	0	1	77.76	1.15	-1.86	High	No	0	0.56	1	1	No
5	0.5	6	108.6	0.03	-1.68	High	No	0	0.55	0	1	No
6	0	4	118.2	2.72	-3.62	High	No	0	0.56	1	3	No
7	0.17	13	289.0	3.92	-6.25	Low	No	3	0.11	1	2	No
9	0.15	9	211.2	2.78	-4.68	Low	No	3	0.11	1	2	No
10	0.29	3	66.3	-0.15	-1.7	High	No	2	0.17	1	1	No
13	0.65	2	97.99	3.6	-4.31	High	No	0	0.56	1	1	No
15	0.06	2	79.9	3.35	-4.14	High	No	0	0.55	0	0	No
16	0.16	8	133.5	2.69	-3.66	High	No	0	0.55	1	3	No
17	0.1	3	66.76	1.48	-2.1	High	Yes	0	0.55	1	2	No
18	0	1	78.76	1.34	-1.86	High	No	0	0.56	1	1	No
19	0.41	4	134.9	1.48	-3.48	High	No	0	0.55	0	0	No

288 [*]Cp. Compound no., Fr. C3: Fraction Csp^3 , R.b.: Rotatable bonds, E. l: ESOL logs, GI abs.: absorption, BBB P. BBB permeability, L.V. Lipinski

289 violations, B.s.: bioavailability score, P.a. PAINS alerts, P.a. Brenk alerts, CY: CYP2C19. Inhibitor.

Table S4. Docking results of the isolated compounds from ethyl acetate fraction, tetracaine and lidocaine with the sodium channel protein. Scores are provided in Kcal/mol, along with the main interactions and the corresponding interacting amino acids. In the case of H-bonds, the lengths of the bond is provided in angstrom, and the role of the compound is mentioned (donor/acceptor).

Compound	Score (Kcal/mol)	Type of interaction	Main interacting amino acid	Length of the bond (angstrom)	Role of ligand in in case of H-bond
Tetracaine	--6.0	H-bond	Gln 249	2.92	Acceptor
Acacetin	-5.7	hydrophobic	PHE 315	NA	NA
			GLN 249		
Acacetin-7-O-glucoside	-7.0	H-bond	ASN 315	3.12	Acceptor
		π-H	GLN 249	3.48	NA
Prunin	-9.0	H-bond	GLN 249	2.95	Acceptor
		π-H	PHE 315	4.19	NA
Apigenin-7-O-rutinoside	-8.2	H-bond	CYS 248	2.9	Donor
		H-bond	ASN 315	3.13	Acceptor
		π-H	LEU 319	4.12	NA
Chlorogenic acid	-6.2	π-H	GLN 249	3.86	NA
citrusin C	-5.8	π-H	PHE 315	4.05	NA
Dehydrodieugenol B	-6.2	mainly hydrophobic	VAL 319	NA	NA
			GLN 249		
			PHE 315		

Didymin	-8.3	H-bond	GLN 249	3.17	Acceptor
		π-H	GLY 249	4.72	NA
lidocaine	-5.3	H-bond	GLN 249	2.76	Acceptor
		π-π	PHE 315	3.92	NA
lithospermic acid	-8.1	π-H	GLN 249	3.77	
methyl caffeate	-4.7	H-bond	SER 315	2.88	Donor
methyl gallate	-4.6	π-H	PHE 315	4.15	NA
		π-H	PHE 315	3.95	
methyl rosmarinate	-7.0	H-bond	CYS 248	4.36	Donor
orientin	-6.6	H-bond	THR 247	2.92	Donor
		H-bond	THR 248	3.38	Donor
		H-bond	GLN 249	3.35	Acceptor
protocatechuic acid	-4.4	H-bond	GLN 249	3.12	Donor
		H-bond	THR 247	3.09	Donor
		π-H	GLN 249	3.65	NA
Rabdosiin	-9.4	H-bond	CYS 248	3.07	Donor
		H-bond	GLN 249	2.98	Acceptor
		π-H	PHE 315	4.1	NA
Rosmanol	-4.9	H-bond	SER 315	2.91	Donor
		H-bond	SER 315	2.6	Donor
		H-bond	PHE 315	3.13	Acceptor

		H-bond	THR 248	3.45	Donor
Rutin	-8.3	π-π	PHE 315	3.88	NA
salvianolic acid F	-5.6	H-bond	THR 247	3	Donor
		H-bond	CYS 248	2.86	Donor
tournefolic acid B	-5.4	H-bond	CYS 248	3.12	Donor
		H-bond	THR 247	3.19	Donor

293

294

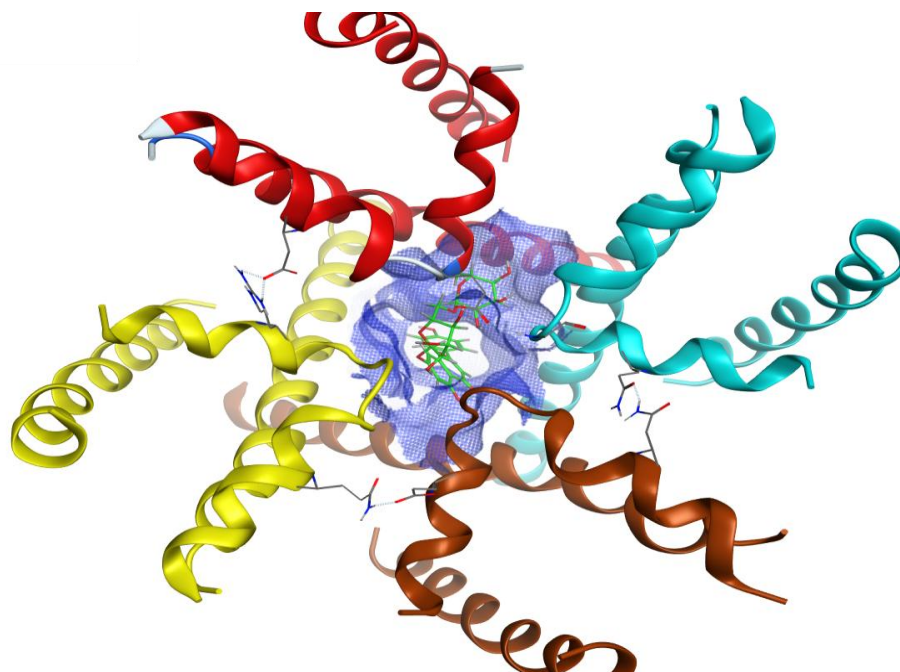295 **Figure S9.** The sodium channel showing Apigenin-7-o-rutinoside in the active site

References

Barros L, Dueñas M, Dias MI, Sousa MJ, Santos-Buelga C, Ferreira IC. 2013. Phenolic profiles of cultivated, in vitro cultured and commercial samples of Melissa officinalis L. infusions. Food chemistry.136:1-8.

Bilal A, Jahan N, Ahmed A, Bilal SN, Habib S, Hajra S. 2012. Phytochemical and pharmacological studies on Ocimum basilicum Linn-A review. International Journal of Current Research and Review.4.

CCGI M. 2016. Molecular Operating Environment (MOE), 2013.08. Chemical Computing Group Inc, Montreal.

Chakraborty A, Devi B, Sanjebam R, Khumbong S, Thokchom I. 2010. Preliminary studies on local anesthetic and antipyretic activities of Spilanthes acmella Murr. in experimental animal models. Indian Journal of Pharmacology.42:277.

Daina A, Michielin O, Zoete V. 2017. SwissADME: a free web tool to evaluate pharmacokinetics, drug-likeness and medicinal chemistry friendliness of small molecules. Scientific reports.7:42717.

Elsayed Y, Refaat J, Abdelmohsen U, Othman E, Stopper H, Fouad M. 2018. Metabolomic profiling and biological investigation of the marine sponge-derived bacterium Rhodococcus sp. UA13. Phytochemical Analysis. 04/19;29.

Estrada-Reyes R, Martinez-Vazquez M, Gallegos-Solís A, Moreno J. 2010. Depressant effects of Clinopodium mexicanum Benth. Govaerts (Lamiaceae) on the central nervous system. Journal of ethnopharmacology. 03/01;130:1-8.

Flegkas A, Milosević Ifantis T, Barda C, Samara P, Tsitsilonis O, Skaltsa H. 2019. Antiproliferative Activity of (-)-Rabdosiin Isolated from Ocimum sanctum L. Medicines.6:37.

Gomes RA, Ramirez RR, Maciel JKdS, Agra MdF, Souza MdFVd, Falcão-Silva VS, Siqueira-Junior JP. 2011. Phenolic compounds from Sidastrum micranthum (A. St.-Hil.) fryxell and evaluation of acacetin and 7, 4'-Di-O-methylisoscutellarein as motulator of bacterial drug resistence. Química Nova.34:1385-1388.

Grayer RJ, Kite GC, Veitch NC, Eckert MR, Marin PD, Senanayake P, Paton AJ. 2002. Leaf flavonoid glycosides as chemosystematic characters in Ocimum. Biochemical systematics and ecology.30:327-342.

Guerrero IC, Andrés LS, León LG, Machín RP, Padrón JM, Luis JG, Delgadillo J. 2006. Abietane diterpenoids from Salvia pachyphylla and S. clevelandii with cytotoxic activity against human cancer cell lines. Journal of natural products.69:1803-1805.

Ibrahim AH, Attia EZ, Hajjar D, Anany MA, Desoukey SY, Fouad MA, Kamel MS, Wajant H, Gulder TAM, Abdelmohsen UR. 2018. New Cytotoxic Cyclic Peptide from the Marine Sponge-Associated Nocardiopsis sp. UR67. Marine drugs.16:290.

Leal F, Taghouti M, Nunes F, Silva A, Coelho AC, Matos M. 2017. Thymus Plants: A Review—Micropropagation, Molecular and Antifungal Activity. Active ingredients from aromatic and medicinal plants.107-126.

Martins N, Barros L, Santos-Buelga C, Henriques M, Silva S, Ferreira IC. 2014. Decoction, infusion and hydroalcoholic extract of Origanum vulgare L.: different performances regarding bioactivity and phenolic compounds. Food Chemistry.158:73-80.

Mimica-Dukic N, Bozin B. 2008. Mentha L. species (Lamiaceae) as promising sources of bioactive secondary metabolites. Current Pharmaceutical Design.14:3141-3150.

342 Mondal S, Mirdha BR, Mahapatra SC. 2009. The science behind sacredness of Tulsi
343 (Ocimum sanctum Linn.). Indian J Physiol Pharmacol.53:291-306.
344 Pereira OR, Peres AM, Silva AM, Domingues MR, Cardoso SM. 2013. Simultaneous
345 characterization and quantification of phenolic compounds in Thymus x citriodorus
346 using a validated HPLC–UV and ESI–MS combined method. Food research
347 international.54:1773-1780.
348 Sharma P, Prakash O, Shukla A, Singh Rajpurohit C, G Vasudev P, Luqman S, Kumar
349 Srivastava S, Bhushan Pant A, Khan F. 2016. Structure-activity relationship studies on
350 holy basil (Ocimum sanctum l.) based flavonoid orientin and its analogue for
351 cytotoxic activity in liver cancer cell line Hepg2. Combinatorial chemistry & high
352 throughput screening.19:656-666.
353 Shoeb M, Jaspars M, MacManus SM, Celik S, Nahar L, Kong-Thoo-Lin P, Sarker SD.
354 2007. Anti-colon cancer potential of phenolic compounds from the aerial parts of
355 Centaurea gigantea (Asteraceae). Journal of natural medicines.61:164.
356 Singh D, Chaudhuri PK. 2018. A review on phytochemical and pharmacological
357 properties of Holy basil (Ocimum sanctum L.). Industrial Crops and
358 Products.118:367-382.
359 Suzuki A, Shirota O, Mori K, Sekita S, Fuchino H, Takano A, Kuroyanagi M. 2009.
360 Leishmanicidal active constituents from Nepalese medicinal plant Tulsi (Ocimum
361 sanctum L.). Chemical and Pharmaceutical Bulletin.57:245-251.
362 Tada H, Murakami Y, Omoto T, Shimomura K, Ishimaru K. 1996. Rosmarinic acid and
363 related phenolics in hairy root cultures of Ocimum basilicum.
364 Phytochemistry.42:431-434.
365 Tawfike A, Attia EZ, Desoukey SY, Hajjar D, Makki AA, Schupp PJ, Edrada-Ebel R,
366 Abdelmohsen UR. 2019. New bioactive metabolites from the elicited marine sponge-
367 derived bacterium Actinokineospora spheciospongiae sp. nov. AMB Express.9:12.
368 Tikhonov DB, Zhorov BS. 2017. Mechanism of sodium channel block by local
369 anesthetics, antiarrhythmics, and anticonvulsants. The Journal of general
370 physiology.149:465-481.
371 Yu Y, Xing N, Xu X, Zhu Y, Wang S, Sun G, Sun X. 2019. Tournefolic acid B, derived
372 from Clinopodium chinense (Benth.) Kuntze, protects against myocardial
373 ischemia/reperfusion injury by inhibiting endoplasmic reticulum stress-regulated
374 apoptosis via PI3K/AKT pathways. Phytomedicine.52:178-186.
375 Zahran EM, Abdelmohsen UR, Hussein AS, Salem MA, Khalil HE, Yehia Desoukey S,
376 Fouad MA, Kamel MS. 2019. Antiulcer potential and molecular docking of flavonoids
377 from Ocimum forskolei Benth., family Lamiaceae. Natural product research.1-5.
378 https://doi.org/10.1080/14786419.2019.1645662

379